An Improved Calibration Framework for Electromagnetic Tracking Devices

Milan Ikits[1,2]   J. Dean Brederson[1,2]   Charles D. Hansen[1,2]   John M. Hollerbach[2]

[1]*Scientific Computing and Imaging Institute,* [2]*School of Computing*
University of Utah
50 Central Campus Drive Rm 3490
Salt Lake City, UT 84112-9205, USA
{ikits, jdb, hansen, jmh}@cs.utah.edu

Abstract

Electromagnetic trackers have many favorable characteristics but are notorious for their sensitivity to magnetic field distortions resulting from metal and electronic equipment in the environment. We categorize existing tracker calibration methods and present an improved technique for reducing static position and orientation errors inherent to these devices. A quaternion based formulation provides a simple and fast computational framework for representing orientation errors. Our experimental apparatus consists of a 6DOF mobile platform and an optical position measurement system, allowing collection of full pose data at nearly arbitrary orientations of the receiver. A polynomial correction technique is applied and evaluated using a Polhemus Fastrak resulting in a substantial improvement of tracking accuracy. Finally, we apply advanced visualization algorithms to give new insight into the nature of the magnetic distortion field.

1   Introduction

Electromagnetic tracking systems have been used extensively in virtual reality research and applications. They determine the position and orientation of a receiver relative to a transmitter by generating and measuring orthogonal electromagnetic fields [20, 14]. These systems are preferable to other tracking technologies because they are relatively inexpensive, cover a reasonably large workspace, provide fairly good resolution with acceptable jitter, convenience of use, and do not suffer from line of sight problems [5]. However, their accuracy is seriously degraded by magnetic field distortions due to metal and electronic equipment located in the environment. The error between the actual and reported position and orientation of the receiver increases in propor-tion to its distance from the transmitter. In fact, position errors can be as high as several feet which limits the usable range of these devices [7].

In the past decade, researchers have proposed a number of methods to improve magnetic tracking accuracy by measuring and compensating for the field distortions. Calibration is possible provided that the magnetic excitation vectors produced by the transmitter remain linearly independent within the working range of the device [20]. All the reported calibration methods collect a number of measurements in the workspace from which error corrections are derived. We categorize these previous approaches based on the correction technique applied, the metrology system used, and the number of DOF calibrated.

1.1   Error Correction Technique

A crucial component of tracker calibration is the method of deriving error corrections from the experimental data. Existing calibration methods implement one or more error correction techniques from the following categories:

- **Analytical**: These techniques assume that the distortion is a function of the receiver position that can be closely approximated by a higher order polynomial. This approach was originally proposed by [20] and later evaluated in [3, 12]. Since it has been shown that the tracker noise is proportional to the fourth power of the transmitter-receiver separation distance [17], the use of approximating polynomials with about the same degree is physically appropriate and has proven to work reasonably well.

- **Global interpolation**: Instead of fitting an analytical model to the collected data, global methods apply scattered data interpolation techniques to describe the distortion field explicitly [22] or to construct a lookup table (LUT) for local interpolation [4].

- **Local interpolation**: Local methods are based on a uniformly spaced LUT from which the error correction is calculated using trilinear interpolation. A uniform calibration table can be built in the distorted tracker space from a systematic measurement procedure [7] or by resampling the irregular dataset onto a rectilinear grid [16, 4, 2]. A more direct approach is to construct the table in the actual workspace [3, 13], in which case fast interpolation and grid traversal algorithms are required to calculate the correction values at runtime. The efficacy of these methods depends on the granularity of the table, because the distortion is assumed to be linear within a grid cell. Comparative studies have shown that local methods perform at least as well as analytical approaches, but their complexity is higher [3, 13].

1.2 Experimental Data Collection

Data collection techniques developed in the past differ in achievable accuracy and ease of use. Direct methods are based on an external metrology system registered to the transmitter to determine the exact location of the receiver [7, 16]. Indirect approaches rely on human perception to approximately align the experimental measurement apparatus, which is typically a platform [22, 12], pegboard [3], or jig [2]. Such methods are generally unsuitable for measuring orientation, but it is possible to determine orientation distortion from a set of constrained poses [13]. Approximate corrections can also be obtained by superimposing real and virtual targets located in the workspace [4].
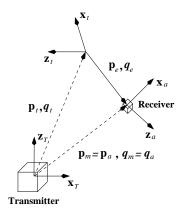
1.3 Position vs. Full Pose

Until recently, research has been focused on correcting the position component of the error only. However, it has been noted that orientation correction is necessary for hand tracking to reduce user confusion and frustration, especially for manipulation tasks [22]. Initial research to correct orientation errors concluded that the orientation error is a function of the receiver position *and* orientation, thus any correction technique is impractical because of the large number of data points required [16]. On the contrary, recent work has shown that orientation correction is possible with reported results comparable to those obtained by position correction techniques [6, 12, 13].

1.4 Contributions

We add to this research area by formulating an improved mathematical framework for orientation correction. In addition, we describe an accurate measurement apparatus consisting of a 6DOF, non-metallic, mobile platform and an optical position tracking system. This apparatus allows full pose data collection at nearly arbitrary orientations over the range of the tracked volume, in a manner similar to [16]. The outcome of our experiments supports the assumption that the orientation error depends on the reported location only [13]. We apply and evaluate a polynomial based correction technique to reduce the effects of magnetic field distortion in a semi-immersive virtual environment comprised of a Fakespace Immersive Workbench and a Polhemus Fastrak. Finally, we explore the nature of tracker distortion using advanced vector field visualization algorithms.

2 The Calibration Problem

The goal of magnetic tracker calibration is to measure and characterize the relationship between the actual receiver position $\mathbf{p}_a$ and orientation $\boldsymbol{q}_a$ and those reported by the tracker, $\mathbf{p}_t$ and $\boldsymbol{q}_t$ (Figure 1). This is done by placing the receiver at a number of known locations in the tracked workspace and measuring its position and orientation, $\mathbf{p}_m$ and $\boldsymbol{q}_m$, with respect to a common reference frame attached to the transmitter. We assume that the measured pose closely matches the actual one or their difference is small enough relative to the distortion that we consider them equal, $\mathbf{p}_m = \mathbf{p}_a$ and $\boldsymbol{q}_m = \boldsymbol{q}_a$.

Figure 1. The calibration error is defined as the difference between the measured and reported receiver position and orientation.

Position error is generally defined as the vector difference between the measured and reported positions:

$$\mathbf{p}_e = \mathbf{p}_m - \mathbf{p}_t \tag{1}$$

Orientation error is not as straightforward to define, because there is no representation that is both minimal and provides an intuitive, nonsingular metric for optimization. Euler angles are a minimal representation but suffer from singularities, while rotation matrices and quaternions are

both redundant and subject to parameter constraints. Fortunately, orientation errors observed with magnetic tracking systems are small, e.g. $< 30^o$ uncorrected and $< 10^o$ corrected, implying that a reduced representation can be used.

2.1 Representation of Orientation Errors

In previous work orientation errors were formulated from the rotation matrix or quaternion relating the reported and measured orientation of the receiver. Euler angle corrections are obtained by sampling the receiver in the same orientation as the transmitter in [12]. A rotation matrix is computed from the correction angles and is multiplied by the reported orientation to yield the corrected orientation. A similar framework has been developed using a quaternion representation [13].

Orientation error has also been defined as the quaternion difference between a closed loop transformation of the receiver to itself and the identity [16]. The outcome of these experiments suggested that the orientation error depends on not only the receiver position but also the orientation. However, careful investigation reveals that this error definition is orientation dependent, since a rotation in the world frame has a different form in the receiver frame depending on its orientation. For example, a rotation about the $\mathbf{x}$ axis in the transmitter frame is identical in the receiver frame when they are oriented the same, but becomes a rotation about the $\mathbf{y}$ axis when the receiver is rotated by 90° about the $\mathbf{z}$ axis of the transmitter.

To overcome this problem we define orientation error using quaternion composition and rotation [15]. The measured and reported orientations are related by orientation error quaternion ${}^t\boldsymbol{q}_e$:

$$\boldsymbol{q}_m = \boldsymbol{q}_t \, {}^t\boldsymbol{q}_e \qquad (2)$$

where $\boldsymbol{q}_m$ and $\boldsymbol{q}_t$ are expressed in the transmitter frame, and ${}^t\boldsymbol{q}_e$ is expressed in the tracked receiver frame (Figure 1). Note that in this form the error is orientation dependent. To obtain an orientation independent error quaternion, we have to express $\boldsymbol{q}_e$ with respect to the transmitter frame:

$$\boldsymbol{q}_e = \boldsymbol{q}_t \, {}^t\boldsymbol{q}_e \, \boldsymbol{q}_t^* = \boldsymbol{q}_t \, (\boldsymbol{q}_t^* \, \boldsymbol{q}_m) \, \boldsymbol{q}_t^* = \boldsymbol{q}_m \, \boldsymbol{q}_t^* \qquad (3)$$

where $*$ denotes the quaternion conjugate.

Let us assume that somehow we can approximate the error quaternion with $\boldsymbol{q}_e'$. Then the corrected orientation can be computed by quaternion composition:

$$\boldsymbol{q}_t' = \boldsymbol{q}_t \, (\boldsymbol{q}_t^* \, \boldsymbol{q}_e' \, \boldsymbol{q}_t) = \boldsymbol{q}_e' \, \boldsymbol{q}_t \qquad (4)$$

In contrast, when using Euler angles, one has to convert them to a rotation matrix, extract the rotation axis, express it in the receiver frame, and then formulate the rotation correction matrix. Even when exploiting the composition suggested by (4) one still has to convert the Euler angles to

a rotation matrix and perform matrix multiplication. All of these operations are more complicated than quaternion composition and can easily be sources of numerical error if not done properly.

A disadvantage of quaternions is that they are a redundant parameterization. For example, they have to be normalized when calculated from interpolation or an analytical model to be applied correctly [13]. Experimental data shows that orientation errors are relatively small, so the scalar part of $\boldsymbol{q}_e$ is always close to one. Thus, the vector part of $\boldsymbol{q}_e$ provides the desired minimal representation and the scalar part can be computed from the constraint of unity.

We can show that the quaternion vector part [11] is similar to other representations used in robotics and computer animation by relating $\boldsymbol{q}_e$ to the angle and axis of rotation:

$$\boldsymbol{q}_e = q_e + \mathbf{q}_e = \cos(\frac{\theta}{2}) + \sin(\frac{\theta}{2}) \, \mathbf{k} \qquad (5)$$

If rotation error angle θ is small, $\sin(\frac{\theta}{2}) \approx \frac{\theta}{2}$, and we can approximate the vector part as:

$$\mathbf{q}_e = \sin(\frac{\theta}{2}) \, \mathbf{k} \approx \frac{\theta \, \mathbf{k}}{2} \qquad (6)$$

This approximation is a scaled version of the exponential map [8] and is similarly related to differential orthogonal rotations [9].

2.2 Calibration via Polynomial Fit

Polynomial fit techniques were among the first calibration methods applied and evaluated for correcting magnetic field distortion [3]. Among their advantages are simplicity, robustness, and speed, since only a few parameters need to be stored for computing the error at a given location. Their disadvantages are that they do not provide a good fit for small errors close to the transmitter and are not as accurate for describing local field distortions as LUT methods. The polynomial coefficients can be obtained from a least squares fit that minimizes the difference between the measured errors and those predicted by the calibration model.

A degree r vector polynomial of position $\mathbf{p}$ can be formulated as:

$$\mathbf{f}(\mathbf{c}, \mathbf{p}) = \mathbf{f}(\mathbf{c}, x, y, z) = \sum_{j=1}^{R} \begin{bmatrix} c_{x,j} \\ c_{y,j} \\ c_{z,j} \end{bmatrix} x^{s_j} \, y^{t_j} \, z^{u_j} \qquad (7)$$

where we assume that each term is unique, at most degree r with nonnegative powers ($0 \leq s_j + t_j + u_j \leq r$), and the polynomial is complete, meaning that all combinations of powers are present in the sum. Given these conditions, it can be shown that the number of polynomial terms in (7) is $R = (r+1)(r+2)(r+3)/6$. For example, a degree four polynomial has 35 unique terms.

Our goal is to find a coefficient vector $\mathbf{c}$ such that the fitted polynomial closely approximates the calibration error at the measurement locations. For position errors this can be written as the minimization of the following objective function:

$$S_p = \sum_{i=1}^{N} \|\mathbf{p}_e^i - \mathbf{f}(\mathbf{c}_p, \mathbf{p}_t^i)\|^2 \qquad (8)$$

where N is the number of data points collected, $\mathbf{p}_t^i$ is the position reported by the tracker, and $\mathbf{p}_e^i$ is the position error at measurement location i defined by (1). This is a linear least squares problem and has a well known closed-form solution [19]. Note that (8) is an over-determined system of equations if and only if $N > R$, meaning that more measurements than the number of polynomial terms are necessary to minimize S_p.

For orientation we formulate the parameter estimation problem as finding the minimum of:

$$S_q = \sum_{i=1}^{N} \|\Delta\mathbf{q}^i\|^2 = \sum_{i=1}^{N} \|\mathbf{q}_e^i - \mathbf{f}(\mathbf{c}_q, \mathbf{p}_t^i)\|^2 \qquad (9)$$

where $\mathbf{q}_e^i$ is the vector part of the error quaternion obtained from (3) at measurement location i. Hence, we treat orientation errors similarly to position errors. Alternative definitions for $\Delta\mathbf{q}^i$ include the vector part of the quaternion that rotates between the fitted and measured error quaternions and the error vector obtained from differential orthogonal rotations. We experimented with these approaches but did not find any significant difference in the calibration results. Since (9) yields a linear problem while the other methods require the use of iterative nonlinear parameter estimation algorithms, we chose the simpler definition.

3 Experimental Apparatus

A good experimental apparatus provides both position and orientation measurements that are sufficiently accurate to not degrade the efficacy of the error correction technique. The apparatus should cover the desired tracking space and not induce further distortions in the magnetic field. Optical measurement systems are the most suitable for this purpose; they do not use mechanical linkages, such as digitizing arms, and have higher accuracy than alternative technologies, such as ultrasonic range measurement. In addition, they can easily establish a precise transformation between the tracker frame and the frame of the display surface.

We used an NDI Optotrak 3020 position tracking system which measures the position of active infrared markers with a nominal accuracy of 0.05 mm per meter of distance along the central focal axis [18]. A non-metallic platform was constructed for mounting the receiver along with six Optotrak markers (Figure 2). The markers were mounted
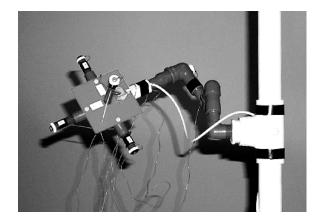

Figure 2. Experimental platform used for data collection. Markers are mounted in six directions around the receiver.

in positive and negative directions along approximately orthogonal axes, such that at least three markers are visible by the camera system at a time. The platform was designed to be mobile with rotational redundancy so that achieving arbitrary orientations is possible throughout the workspace. Samples were taken independently from the tracker and the Optotrak, and we verified that the placement of the markers does not distort the magnetic field. Two techniques were developed in support of the apparatus: one for estimating the fixed geometric relationship between the transmitter and the Optotrak, and the location of the markers relative to the receiver, and another for extracting the receiver pose from three simultaneous optical position measurements.

3.1 Kinematic Model

The measurement apparatus can be described by a kinematic model (Figure 3) which relates the actual receiver pose to the marker positions expressed by the following set of equations:

$$\mathbf{v}_j = \mathbf{p}_0 + \mathbf{R}(\boldsymbol{q}_0)(\mathbf{p} + \mathbf{R}(\boldsymbol{q})\,\mathbf{r}_j) \quad j = 1\ldots 6 \qquad (10)$$

where $\mathbf{p}_0$ and $\boldsymbol{q}_0$ define the transformation between the Optotrak and transmitter frames, $\mathbf{r}_j$ is the location of marker j in the receiver coordinate system, $\mathbf{p}$ and $\boldsymbol{q}$ are the actual position and orientation of the receiver, $\mathbf{v}_j$ is the position of marker j as a function of the receiver pose, and $\mathbf{R}(\boldsymbol{q})$ is an operator which converts a quaternion to a rotation matrix [15]. Since only three marker measurements are used at a particular location, we have a reduced set of equations:

$$\mathbf{y}^i = \begin{bmatrix} \mathbf{v}_{j_1}^i \\ \mathbf{v}_{j_2}^i \\ \mathbf{v}_{j_3}^i \end{bmatrix} = \mathbf{y}^i(\boldsymbol{\phi}, \mathbf{p}^i, \boldsymbol{q}^i) \quad i = 1\ldots N \qquad (11)$$

where $j_1, j_2, j_3 \in [1 \ldots 6]$ are the indices of the markers visible by the Optotrak, and the fixed geometric parameters are collected into a parameter vector ϕ:

$$\phi = \begin{bmatrix} \mathbf{p}_0 \\ \boldsymbol{q}_0 \\ \mathbf{r}_1 \\ \vdots \\ \mathbf{r}_6 \end{bmatrix} \qquad (12)$$

Since we cannot know ϕ in advance, we have to estimate it by effectively registering the transmitter location to the Optotrak and the marker positions in the receiver frame. Thus, we collected 20 measurements in close proximity of the source where the field distortions can be assumed to have a minimal effect on the parameter estimates. Since the optical measurements are more accurate than the data collected from the tracker, we implemented a version of a total least squares estimation technique [21], which takes into account the input noise present in the kinematic system described by (11). We verified the validity of our results via the χ^2 statistic [19] obtained after the fit and concluded that our *a priori* assumptions about the noise model were appropriate. We also examined the *a posteriori* covariance matrix of the parameter estimates, which indicated that the estimation error had a standard deviation of 0.15 mm, the nominal accuracy of the Optotrak measurements in our setup. Additional details on this technique can be found in Appendix A.
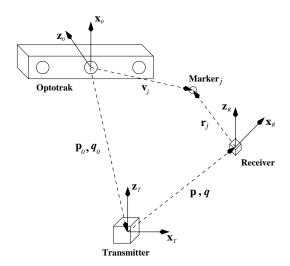

Figure 3. Kinematic model of the apparatus.

The use of quaternions as a redundant set of parameters in both ϕ and input measurements $\boldsymbol{q}^i$ causes problems with the estimation procedure, because they must be renormalized at every iteration. Unfortunately, we found that this renormalization prohibits convergence of the algorithm. The problem can be avoided by including the calculation

of the largest magnitude component in the kinematic equations. Thus, we need an operator $\boldsymbol{q}(\mathbf{s})$ that converts three quaternion elements to a unit quaternion:

$$\mathbf{v}_j = \mathbf{p}_0 + \mathbf{R}(\boldsymbol{q}(\mathbf{s}_0))(\mathbf{p} + \mathbf{R}(\boldsymbol{q}(\mathbf{s}))\,\mathbf{r}_j) \quad j = 1 \ldots 6 \quad (13)$$

It can be shown that the Jacobian $\partial\boldsymbol{q}/\partial\mathbf{s}$ is well-conditioned as long as $\mathbf{s}$ is the minimum magnitude part of $\boldsymbol{q}$ (Appendix B). To satisfy this condition, the system is dynamically reparameterized at each iteration of the estimation procedure, which is similar to the method suggested for the exponential map in [8].

3.2 Pose Extraction

When the vector of fixed geometric parameters ϕ is known, the position $\mathbf{p}^i$ and orientation $\mathbf{s}^i$ of the receiver at measurement location i can be computed from the three marker positions $\mathbf{y}^i$ by finding the inverse of (13). Although an analytical solution exists, it is unclear how it behaves numerically when the location of the markers are not known precisely. Hence, we chose to use an iterative estimation procedure which finds the pose by minimizing the error between the predicted and measured marker positions. Good initial estimates are provided by the uncorrected tracker readings and convergence is achieved in a few iterations.

4 Results

A total of 600 measurements were collected within a $1.8\,\mathrm{m} \times 1.5\,\mathrm{m} \times 0.9\,\mathrm{m}\,(6\,' \times 5\,' \times 3\,')$ volume located above and in front of the display surface of the workbench. Possible sources of distortion included metal reinforcement in the floor (0.8 m below the transmitter), a metal door (2.1 m away from the transmitter), and several CRT displays (at least 1.8 m away from the transmitter). The collection of 480 calibration poses was based on a $12 \times 10 \times 5$ grid with a 0.15 m (6″) cell size. In addition, 120 validation measurements were taken randomly in the workspace. We randomized the orientation of the receiver to ensure that it covered the space of possible rotations. At each pose, we took 120 samples from the tracker and 100 samples from the Optotrak and calculated their mean and standard deviation. Only two calibration poses had to be rejected because of unreasonably large deviations in the optical measurements.

We fit degree four polynomials to the position and orientation errors computed from the calibration measurements. The performance of the polynomial fit was evaluated using the validation dataset. Statistical measures were computed from the position error magnitudes and orientation correction angles before and after calibration (Table 1). The results indicate that position errors have been reduced by almost 90 % on average, whereas for orientation errors the reduction is slightly less, at around 80 % on average.

Position error

Measure (mm)	Original	Corrected	Improvement
Mean	42.3	4.82	88.6 %
Standard dev.	26.3	4.04	84.7 %
Maximum	97.5	22.8	76.6 %

Orientation error

Measure (deg)	Original	Corrected	Improvement
Mean	4.72	0.93	80.3 %
Standard dev.	2.51	0.50	80.1 %
Maximum	10.71	2.09	80.5 %

Table 1. Results of error correction.

Scatter plots of the error magnitude as a function of the transmitter-receiver separation distance (Figures 4 and 5) show that overall the polynomial fit correction is quite effective, but does not improve accuracy within a 0.5 m radius volume of space around the source. This problem is attributed to the global nature of the correction technique [3, 12].
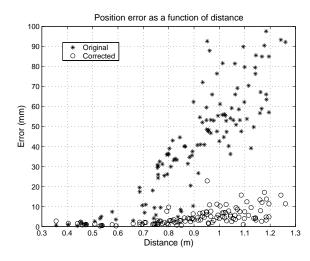
Figure 4. Position error magnitude as a function of distance before and after calibration.

5 Visualization of Field Distortion

In the past several methods have been used for visualizing the effect of the magnetic field distortion on the position error, including iconic representations [3, 16] and grid visualization [22, 6]. Scatter plots and histograms provide quantitative information about the distortion field, but tell nothing about its shape and structure. Since all of the proposed techniques are based directly on the collected data,
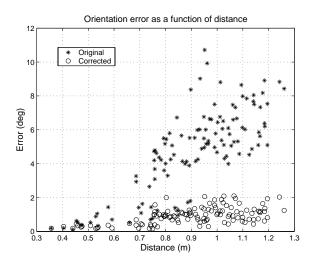
Figure 5. Orientation error angle as a function of distance before and after calibration.

the quality of the visualization depends on the resolution of the sampled space.

We investigated the use of illuminated streamlines as a global visualization technique with additional local shading information [23]. A number of seed points were chosen randomly in the x-y plane of the transmitter and streamlines were advected in the direction of the distortion field, which is described by the fitted polynomial (Figure 6). The intensity and opacity of the line segments are varied according to the local magnitude of the field. The figure clearly shows the axially symmetric shape of the position distortion without visual clutter [3].
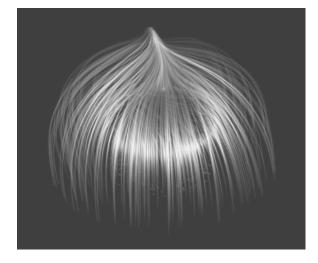
Figure 6. Illuminated streamlines visualize the shape of the distortion field.

To study the nature of orientation distortion, we plotted icons representing orientation error vectors at measurement locations in an x-y slice of the calibration dataset (Figure 7). The icon magnitude is related to the orientation error angle via a logarithmic transfer function, and the direction corresponds to the axis of rotation. Icons with larger magnitudes form a circular pattern around the transmitter. This indicates a functional relationship between the orientation error and the position of the receiver independent of its orientation. Smaller icons appear randomly oriented, probably because their magnitudes approach the accuracy of the measurement apparatus.
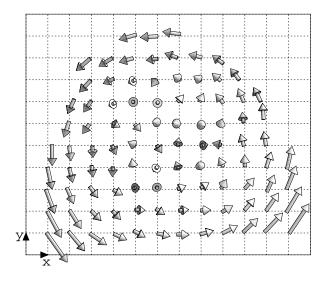

Figure 7. An x-y slice of the orientation error vectors collected near the transmitter.

6 Conclusions and Future Work

Accurate position and orientation tracking is an important component of immersive and semi-immersive virtual environments. The accuracy of magnetic tracking systems can be improved significantly by measuring and compensating for the magnetic field distortions. Analytical techniques use a higher order polynomial to characterize the distortion without increasing the effective tracker latency. For example, the correction of both position and orientation errors in our VE setup takes approximately $18\,\mu s$ on a MIPS R10000 processor.

The polynomial coefficients are found by minimizing the difference between the measured errors and those predicted by the calibration model. Numerical conditioning of the parameter estimation is an important issue, which was not addressed in this work. A better fit might be obtained by excluding poorly identifiable parameters from the estimation procedure [9].

It is unclear how well the correction methods perform when compared to each other. Experimental results indicate that polynomial techniques increase the distortion in proximity of the transmitter. Possible future enhancements include analytical models derived directly from the operating principles of magnetic tracking devices and the combination of local and global correction methods.

We intend to verify our approach with other tracking systems, such as an Ascension Flock of Birds with an Extended Range Transmitter. The tedious data collection procedure can be accelerated by manually posing the apparatus, but this yields less accurate optical measurements.

Advanced visualization algorithms provide additional information about the nature of the magnetic distortion field. We are currently developing interactive techniques based on combined visual and haptic modes for the exploration of vector data sets [1]. Hopefully, these techniques will grant us further insight into the tracker calibration problem and suggest future research directions.

Acknowledgments

A Using Total Least Squares to Estimate ϕ

The total least squares formulation for estimating ϕ minimizes the normalized measurement errors in the following form [21]:

$$\chi^2 = \sum_{i=1}^{N} \left[\begin{array}{c} \mathbf{x}^i - \hat{\mathbf{x}}^i \\ \mathbf{y}^i(\phi, \mathbf{x}^i) - \hat{\mathbf{y}}^i \end{array} \right]^T \mathbf{V}_i^{-1} \left[\begin{array}{c} \mathbf{x}^i - \hat{\mathbf{x}}^i \\ \mathbf{y}^i(\phi, \mathbf{x}^i) - \hat{\mathbf{y}}^i \end{array} \right] \tag{14}$$

where:

$$\mathbf{x}^i = \left[\begin{array}{c} \mathbf{p}^i \\ \mathbf{s}^i \end{array} \right] \tag{15}$$

are estimates of the input measurements $\hat{\mathbf{x}}_i$ included as parameters augmenting ϕ. Recall that $\mathbf{y}^i$ is a function of the receiver pose (11) and the output measurement vector $\hat{\mathbf{y}}^i$ contains the reported Optotrak positions.

Since the measurement errors are assumed to be independent and normally distributed with zero mean, the error covariance matrices $\mathbf{V}_i$ take the following form:

$$\mathbf{V}_i = \mathbf{V} = \left[\begin{array}{cc} \mathbf{V}_x & \mathbf{0} \\ \mathbf{0} & \mathbf{V}_y \end{array} \right] \tag{16}$$

where $\mathbf{V}_x$ and $\mathbf{V}_y$ represent the noise in the input and output measurements. Usually $\mathbf{V}_x$ and $\mathbf{V}_y$ are diagonal matrices containing the variances of the measurements

σ_x^2 and σ_y^2, respectively. Goodness of fit is tested by examining χ^2 from (14) with the converged values of $\mathbf{x}^i$ and ϕ. It can be shown that if the Gaussian assumptions are valid, then χ^2 has an expected value of $\nu = Nm - M$ with a standard deviation of $\sqrt{2\nu}$, where m is the number of elements in $\mathbf{y}^i$ and the system has M parameters [19]. Another confidence test can be performed by finding an estimate of the *a posteriori* parameter error covariance matrix. More details on this method and its applications can be found in [10].

B Operator $q(\mathbf{s})$

Without loss of generality we can assume that the largest magnitude element of $\boldsymbol{q} = \begin{bmatrix} q_0 & q_1 & q_2 & q_3 \end{bmatrix}^T$ is q_0. Then:

$$\mathbf{s} = \begin{bmatrix} q_1 \\ q_2 \\ q_3 \end{bmatrix} \qquad (17)$$

Since valid rotations are represented by unit quaternions, we calculate q_0 as:

$$q_0 = \pm\sqrt{1 - \mathbf{s}^T\mathbf{s}} = \pm\sqrt{1 - q_1^2 - q_2^2 - q_3^2} \qquad (18)$$

The Jacobian $\partial\boldsymbol{q}/\partial\mathbf{s}$ can be written in the following form:

$$\frac{\partial\boldsymbol{q}}{\partial\mathbf{s}} = \begin{bmatrix} \mp q_1/q_0 & \mp q_2/q_0 & \mp q_3/q_0 \\ 1 & 0 & 0 \\ 0 & 1 & 0 \\ 0 & 0 & 1 \end{bmatrix} \qquad (19)$$

This matrix is well-conditioned as long as q_0 is not close to zero, which is true, since q_0 is assumed to be the largest magnitude element of $\boldsymbol{q}$. The sign of q_0 is fixed until $\boldsymbol{q}$ is reparametrized. Thus, the ambiguity in (18) and (19) can be handled by carrying the sign over from the previous iteration of the estimation procedure.

REFERENCES

[1] J. D. Brederson, M. Ikits, C. Johnson, and C. Hansen. The visual haptic workbench. *Proc. Fifth PHANToM Users Group Workshop*, Aspen, CO, Oct. 2000.

[2] W. Briggs. Magnetic calibration by tetrahedral interpolation. *Proc. NIST-ASME Industrial Virtual Reality Symposium*, MH-5/MED-9, pp. 27–32, Chicago, IL, Nov. 1999.

[3] S. Bryson. Measurement and calibration of static distortion of position data from 3D trackers. *Proc. SPIE Conf. Stereoscopic Displays and Applications III*, pp. 244–255, San Jose, CA, Feb. 1992.

[4] M. Czernuszenko, D. Sandin, and T. DeFanti. Line of sight method for tracker calibration in projection-based VR systems. *Proc. 2nd International Immersive Projection Technology Workshop*, Ames, IA, May 1998.

[5] N. Durlach and A. Mavor, editors. *Virtual Reality: Scientific and Technological Challenges*. National Academy Press, Washington, D.C., 1994.

[6] S. Ellis, S. Adelstein, G. Baumeler, G. Jense, and R. Jacoby. Sensor spatial distortion, visual latency, and update rate effects on 3D tracking in virtual environments. *Proc. IEEE Virtual Reality*, pp. 218–221, Houston, TX, Mar. 1999.

[7] M. Ghazisaedy, D. Adamczyk, D. Sandin, R. Kenyon, and T. DeFanti. Ultrasonic calibration of a magnetic tracker in a virtual reality space. *Proc. IEEE Virtual Reality Annual International Symposium*, pp. 179–188, Research Triangle Park, NC, Mar. 1995.

[8] F. Grassia. Practical parametrization of rotations using the exponential map. *Journal of Graphics Tools*, 3(3):29–48, 1998.

[9] J. Hollerbach and C. Wampler. The calibration index and taxonomy of robot kinematic calibration methods. *International Journal of Robotics Research*, 15(6):573–591, 1996.

[10] M. Ikits. Coregistration of pose measurement devices using nonlinear total least squares parameter estimation. Technical Report UUCS-00-018, School of Computing, University of Utah, Dec. 2000.

[11] A. Katz. Special rotation vectors – a means for transmitting quaternion information in three components. *Journal of Aircraft*, 30(1):148–150, 1993.

[12] V. Kindratenko. Calibration of electromagnetic tracking devices. *Virtual Reality: Research, Development, and Applications*, 4:139–150, 1999.

[13] V. Kindratenko and A. Bennett. Evaluation of rotation correction techniques for electromagnetic position tracking systems. *Proc. Eurographics Workshop on Virtual Environments*, pp. 13–23, Amsterdam, The Netherlands, June 2000.

[14] J. Kuipers. SPASYN – an electromagnetic relative position and orientation tracking system. *IEEE Trans. Instrumentation and Measurement*, IM-29(4):462–466, 1980.

[15] J. Kuipers. *Quaternions and Rotation Sequences*. Princeton University Press, Princeton, NJ, 1999.

[16] M. Livingston and A. State. Magnetic tracker calibration for improved augmented reality registration. *Presence: Teleoperators and Virtual Environments*, 6(5):532–546, 1997.

[17] M. Nixon, B. McCallum, W. Fright, and N. Price. The effects of metals and interfering fields on electromagnetic trackers. *Presence: Teleoperators and Virtual Environments*, 7(2):204–218, 1998.

[18] Northern Digital, Inc. http://www.ndigital.com.

[19] W. Press, S. Teukolsky, W. Vetterling, and B. Flannery. *Numerical Recipes in C*. Cambridge University Press, 2nd edition, 1992.

[20] F. Raab, E. Blood, T. Steiner, and R. Jones. Magnetic position and orientation tracking system. *IEEE Trans. Aerospace and Electronic Systems*, AES-15(5):709–718, 1979.

[21] H. Schwetlick and V. Tiller. Numerical methods for estimating parameters in nonlinear models with errors in the variables. *Technometrics*, 27:17–24, 1985.

[22] G. Zachmann. Distortion correction of magnetic fields for position tracking. *Proc. Computer Graphics International*, pp. 213–220, Belgium, June 1997.

[23] M. Zöckler, D. Stalling, and H. Hege. Interactive visualization of 3D-vector fields using illuminated streamlines. *Proc. IEEE Visualization*, pp. 107–113, San Francisco, CA, Oct. 1996.